


The effect of cosmic web filaments on galaxy evolution

Callum J. O’Kane ^{*}, Ulrike Kuchner ^{*}, Meghan E. Gray and Alfonso Aragón-Salamanca ^{*}

School of Physics and Astronomy, University of Nottingham, Nottingham NG7 2RD, UK

Accepted 2024 September 6. Received 2024 August 14; in original form 2024 May 23

ABSTRACT

Galaxy properties are known to be affected by their environment. This is well established for the extremes of the density scales, between the high-density cluster environment and the low-density field. It is, however, not fully understood how the intermediate-density regime of cosmic web filaments affects galaxy evolution. We investigate this environmental effect using a mass complete sample of 23 441 galaxies in the Sloan Digital Sky Survey DR8 Main Galaxy Sample ($M_{\text{Stellar}} > 10^{9.91} M_{\odot}$). We define six environments, probing different density regimes and representing unique stages in the structure formation process, comparing the differences in star formation activity and morphology between them. We find that galaxies in filaments tend to be less star-forming and favour more early-type morphologies than those in the field. These differences persist when considering stellar mass-matched samples, suggesting that this is a consequence of the environment. We further investigate whether these trends are a result of the large-scale or local environment through constructing samples matched both in stellar mass and local galaxy density. We find that when also matching in local galaxy density, the differences observed between the filament and field population vanishes, concluding that the environmental effect of filaments can be entirely parametrized by a local galaxy density index. We find that differences can still be seen in comparisons with the interiors of clusters, suggesting these are unique environments which can impart additional physical processes not characterized by local galaxy density.

Key words: methods: data analysis – galaxies: evolution – large-scale structure of Universe.

1 INTRODUCTION

Under a cold dark matter cosmological paradigm, the present-day matter distribution is the result of the compounding clustering of dark matter haloes. This is seen in galaxy clusters, maxima of the universal density field and the culmination of the hierarchical formation model. These clusters, and the elongated chains of galaxies called ‘filaments’ which connect them, form a highly complex and anisotropic matter distribution at the megaparsec scale called the Cosmic Web (Bond, Kofman & Pogosyan 1996). The Cosmic Web, described by Zel’dovich formalism (Zel’dovich 1970), comprises of clusters, filaments, sheets, walls, knots, and voids, each representing unique stages of the structure formation process. This large-scale structure (LSS) of the Universe is well established in both theory and observations, with observational signatures detected in many large-scale surveys such as the Sloan Digital Sky Survey (SDSS; York et al. 2000), GAMA (Driver et al. 2009), and 2dFGS (Colless et al. 2001). Filaments of the cosmic web account for a large portion of the universal mass budget, with approximately half of the mass located within filaments despite occupying only 6 per cent of the total volume (Cautun et al. 2014). The role of this LSS in shaping galaxy properties is relatively unknown, and must be considered for a comprehensive theory of galaxy evolution.

The process in which a galaxy truncates its star formation, transitioning from actively star-forming to quiescent, is often called ‘quenching’ and is not entirely understood. This is due to its

complex nature, with numerous different processes often occurring simultaneously to halt star formation. These processes generally fall within two different categories, mass quenching and environmental quenching. Mass quenching refers to internal processes such as active galactic nucleus (AGN) feedback (Croton et al. 2006) and supernova explosions (Larson 1974). Environmental quenching refers to the effect caused by the environment where the galaxy is located, including processes such as ram pressure stripping (Gunn & Gott 1972), strangulation (Larson, Tinsley & Caldwell 1980), and harassment (Moore et al. 1996). It has been found that the effects of mass and the environment appear to be separable up to at least $z = 1$, suggesting that both mass and environmental quenching are independent processes (Peng et al. 2010).

The correlation between galaxy properties, and local galaxy density is well established in the literature. One such example is the morphology–density relation (Dressler 1980), showing that galaxies with early-type morphologies are more abundant in regions of high local galaxy density, such as cluster cores. It is currently unclear as to whether relationships such as the morphology–density and others like it such as colour–density (e.g. Baldry et al. 2006; Bamford et al. 2009) and star formation–density (e.g. Hashimoto et al. 1998; Kauffmann et al. 2004) are driven entirely by processes correlated with local density on small scales or are influenced by the geometry, topology, and physics of the LSS. The multiscale characteristics of the cosmic web means that its components span density scales over many magnitudes (Aragón-Calvo, van de Weygaert & Jones 2010). This means that the different cosmic web components, including cosmic filaments, cannot be defined or identified through density alone.

^{*} E-mail: callum.o'kane@nottingham.ac.uk

Investigations concerning the effect of cosmic web filaments on galaxy properties are gaining momentum. Within the hierarchical formation model, the assembly histories of galaxies are expected to be affected by the past large-scale environment, with intrinsic properties, such as mass, spin, and alignment affected by this history while also correlating with the present environment. Although it is generally agreed that filaments do affect the properties of galaxies to some degree, the mechanisms responsible and their relative contributions are not well known. Many studies find that galaxies closer to filaments are redder in colour with reduced star formation (e.g. Martínez, Muriel & Coenda 2016; Chen et al. 2017; Kraljic et al. 2018; Mahajan, Singh & Shobhana 2018; Singh, Mahajan & Bagla 2020; Castignani et al. 2022b; Parente et al. 2024). For example, Kuutma, Tamm & Tempel (2017) find an elevated elliptical-to-spiral ratio towards filaments, concluding that this may be evidence of an increased merger rate inside filaments, transforming spiral galaxies to ellipticals as they migrate towards clusters. Possibly related to this, Chen et al. (2017) find that close to and inside filaments, galaxies are larger than further away from filaments.

Filaments host large reservoirs of multiphase gas with varying temperatures and densities (Snedden et al. 2016). This extra gas component could affect galaxies in a unique way which cannot be characterized through local galaxy density alone. One such example is shown by Kleiner et al. (2017), who find that the most massive galaxies ($\log(M_{\text{stellar}}/M_{\odot}) > 11$) possess enhanced HI fractions relative to the field population, suggesting that sufficiently massive galaxies can rejuvenate their gas supply through accretion from filaments, an example of ‘Cosmic Web Enhancement’ (Vulcani et al. 2019). Supporting this, other studies report that galaxies in filaments have enhanced rates of star formation (e.g. Fadda et al. 2008; Darvish et al. 2014), although sample sizes, cosmic variance, and different characterizations of the environment certainly make it hard to settle on a conclusion. Furthermore, filamentary cold gas accretion is especially relevant at high redshift during galaxy formation. Studies at higher redshifts such as that of Darvish et al. (2014), investigating filamentary structures at $z = 0.84$, find that, while the median mass and star formation rate of individual star-forming galaxies do not depend on the environment, the fraction of star-forming galaxies is elevated in filaments. The authors propose that mild galaxy–galaxy interactions may be responsible or that this enhancement could be the result of selection biases.

In addition to filamentary accretion, galaxy clusters accumulate a large fraction of their mass through the accretion of galaxy groups (McGee et al. 2009; Dressler et al. 2013); these groups assemble inside filaments and drift towards clusters. During their accretion into cluster cores, galaxies are affected by the cluster’s hot intracluster gas (the intracluster medium, ICM). While it seems evident that galaxies undergo some transformations (that changes galaxies from star-forming late-type galaxy to passive early-type galaxy) as they interact with the ICM (e.g. Gunn & Gott 1972; Nulsen 1982), a transformation could, at least in part, occur before the galaxies reach the cluster. This idea is called ‘pre-processing’ (Fujita 2004), and has gained considerable attention over the past few decades. Two possible environments in which pre-processing may occur are filaments and groups. For example, Donnan, Tojeiro & Kraljic (2022) report an increased gas-phase metallicity for galaxies closer to nodes of the cosmic web relative to those further away, with a similar, weaker trend observed for filaments. Martínez et al. (2016) provide evidence for the scenario that both web components relate to pre-processing. Comparing galaxies in filaments with galaxies undergoing isotropic infall on to clusters, they found that filaments contain a larger fraction

of galaxies with reduced specific star formation rates than those isotropically infalling.

Simulation work has also been employed to understand the impact of filaments better. One such example is Bulichi, Dave & Kraljic (2024) using the Simba simulations to find that at $z = 0$ galaxies within 100 kpc of filaments are significantly suppressed in star formation, a similar result is also seen in EAGLE and IllustrisTNG simulations. The authors conclude that this may be the result of shock-heating within filaments. This is further shown by Hasan et al. (2023), who use IllustrisTNG simulations and find that at $z \leq 0.5$ low-mass galaxies ($8 \leq \log(M_{\text{stellar}}/M_{\odot}) < 9$) are significantly suppressed in star formation within 1 Mpc to filaments, a trend driven mostly by satellite galaxies. This provides further evidence that low-mass galaxies may be more susceptible to environmental quenching compared to higher mass galaxies.

A key unanswered question that our paper addresses, is whether or not the effects of filaments are solely a consequence of the well-established relations with local galaxy density (e.g. morphology–density and star formation–density) or if the physical processes associated with the large-scale cosmic web imparts specific effects. The scale over which one considers densities correlates with different processes; at the smallest scales, density corresponds with the most stochastic and recent processes, whereas larger scales consider the averaged, smooth histories of galaxies (Kraljic et al. 2018). Past studies have attempted to take into account local density through various means, such as number density (Eardley et al. 2015; Kraljic et al. 2018), r -band luminosity density (Kuutma et al. 2017), and the Delaunay Tessellation Field Estimator (Laigle et al. 2018; Galárraga-Espinosa, Garaldi & Kauffmann 2023). It is, however, unclear if galaxy density on small (≤ 1 Mpc) scales can explain the observed trends within filaments. If galaxies in filaments are subject to processes which are not characterized by local galaxy density, signatures of this could manifest as differential effects at constant mass and density.

Observational studies are limited by the available data. Current spectroscopic surveys either lack the necessary depth or spatial extent for a robust investigation of pre-processing in the vicinity of galaxy clusters. As such, the majority of past studies are restricted to large-scale surveys (e.g. SDSS). While they offer large statistical samples, they generally suffer from relatively low sampling rates. Conversely, higher sampling in dedicated studies investigating pre-processing of individual clusters is currently restricted to only the most nearby ones, such as the Virgo cluster (e.g. Chung et al. 2021; Castignani et al. 2022a,b; Brown et al. 2023). To address these requirements, we must look ahead to the next generation of spectroscopic surveys. One such survey of note is the WEAVE Wide-Field Cluster Survey (WWFCS; Kuchner et al., in preparation) utilizing the WEAVE (WHT Enhanced Area Velocity Explorer) multi-object spectrograph on the William Herschel Telescope (Dalton et al. 2014; Jin et al. 2023). The WWFCS will systematically observe 16–20 galaxy clusters in the nearby Universe ($z \sim 0.05$) out to $5R_{200}$, measuring thousands of optical spectra per cluster down to a total magnitude limit of $r \approx 19.75$, corresponding to a stellar mass limit $\log(M_{\text{stellar}}/M_{\odot}) \approx 9$. The large spatial coverage with deep observations will prove invaluable in studies of the environmental effects of the cosmic web around galaxy clusters.

This paper serves as a preliminary investigation to the WWFCS, taking a step towards answering the question of local density versus LSS in the context of environmental quenching, with the currently available data. We explore the effect of cosmic web filaments on galaxy properties in the SDSS DR8 Main Galaxy Sample, using DISPERSE (Sousbie 2011) to map the projected filament network.

Table 1. A description of the three regions considered in this work. (1) Name of the region used throughout this work. (2) Name of the WWFCS targets within the regions. (3) Redshift of the cluster. (4) Right ascension of the cluster (J2000). (5) Declination of the cluster (J2000). (6) [Min, Max] redshift of the region. (7) Right ascension of region centre. (8) Declination of the region centre. (9) [Min, Max] box coordinates in angular coordinates $(\alpha - \alpha_{\text{centre}}) \cos \delta$. (10) [Min, Max] box coordinates in angular coordinates $(\delta - \delta_{\text{centre}})$. (11) Number of galaxies in the region following the cuts detailed in Section 2.

Region ¹	A		B		C	
WWFCS target name ²	Z2844	RX1022	A1668	A1795	A1831	A2124
z_{cluster} ³	0.050	0.055	0.063	0.063	0.063	0.067
α_{cluster} ⁴	150.65°	155.54°	195.94°	207.21°	209.81°	236.24°
δ_{cluster} ⁵	32.71°	38.53°	19.27°	26.59°	27.98°	36.11°
z ⁶	[0.0425, 0.0625]		[0.053, 0.073]		[0.057, 0.077]	
α_{centre} ⁷	153.09°		202.88°		236.24°	
δ_{centre} ⁸	35.61°		23.62°		36.11°	
$(\alpha - \alpha_{\text{centre}}) \cos \delta$ ⁹	[-16.376°, 16.376°]		[-18.207°, 18.207°]		[-10.706°, 10.706°]	
$(\delta - \delta_{\text{centre}})$ ¹⁰	[-16.964°, 16.964°]		[-15.693°, 15.693°]		[-10.706°, 10.706°]	
N ¹¹	6201		11547		5693	

We anchor our investigation around six of the target clusters planned to be observed in the WWFCS with sufficient coverage by SDSS. The SDSS is ideal for such studies as it is thoroughly complete at this redshift range while spanning a large angular size of 7966 deg². Although it does not reach the depth and sampling density of the planned WWFCS, it allows us to cover very large areas with a homogeneous data set to explore a broad range of environments. We define six distinct environments and test differences in star formation activity and morphology, investigating how these differences vary in samples matched in stellar mass only, and samples matched both in stellar mass and local galaxy density.

This paper is outlined as follows. Section 2 outlines the data and the sample selection used in this work. Section 3 presents the main methodology, including the mapping of filaments, the star formation suppression metric that we use to characterize star formation activity, the definition of local densities, and the environmental classification scheme. Results are presented and discussed in Section 4, with conclusions and future extensions presented in Section 5.

Throughout this work, we adopt the *WMAP* 9 cosmology (Hinshaw et al. 2013), with $H_0 = 69.32 \text{ km s}^{-1} \text{ Mpc}^{-1}$. All statistical errors are determined via bootstrapping, such that the error corresponds to the standard deviation of the distribution of the target quantity calculated in 1000 subsamples of the parent, while allowing for replacement.

2 DATA

In this work, we select galaxies from the SDSS Data Release Eight (DR8; Aihara et al. 2011) belonging to the Main Galaxy Sample.¹ We select galaxies from the Main Galaxy sample with `class = ‘GALAXY’` and `zWarning = 0 or 16`, indicating reliable redshifts. We further limit our sample to galaxies with an extinction-corrected apparent r -band petrosian magnitude r_{petro} less than 17.77, corresponding to the completeness limit of the SDSS Main Galaxy Sample (Strauss et al. 2002).

2.1 Galaxy sample

This investigation is motivated by the WWFCS, exploring what may be inferred from existing data over larger spatial scales, both to

¹ While the Main Galaxy Sample was first observed and released in DR7 and the sample is practically unchanged in DR8, we query galaxies from DR8 to utilize the reprocessed photometry as well as the availability to retrieve the MPA–JHU spectral measurements (see Section 2.3) from SDSS directly.

identify the current state of knowledge and as a measure to build upon. We therefore choose to anchor our investigation and galaxy sample around the WWFCS target clusters. These target clusters consist of galaxy clusters that have previously been observed in the WINGS (Fasano et al. 2006) and OmegaWINGS (Moretti et al. 2017) surveys. These WINGS clusters cover a wide range of velocity dispersions, X-ray luminosities, and virial masses ($\sigma = 500\text{--}1200 \text{ km s}^{-1}$; $\log L_X = 43.3\text{--}45.0 \text{ erg s}^{-1}$; $\log_{10}(M/M_\odot) = 13.8\text{--}15.5$). The WWFCS cluster targets are selected such that they possess statistically indistinguishable velocity dispersion and X-ray luminosity distributions from the parent WINGS sample, forming an unbiased sample in terms of their mass distribution.

Of the 16 WWFCS targets, 12 reside within the SDSS Main Galaxy sample footprint. Given the reduced number density of SDSS galaxies compared to the number density which will be observed in the WWFCS, we must observe larger spatial scales to accommodate for the reduced statistics. Motivated by this, we initially select galaxies within a $100 \times 100 \text{ Mpc}^2$ area centred on the WWFCS targets, within a redshift range $\Delta z = \pm 0.01$ centred on the cluster redshift. Of the 12 targets, only 6 reside at least 50 Mpc away from the main galaxy sample footprint edges, allowing for the above selection to occur. Since there is some overlap between these six areas, to avoid including duplicate galaxies, we opt to merge the overlapping areas, resulting in three unique regions of different sizes with a depth of $\Delta z = 0.02$, labelled A, B, and C. The resulting regions, as well as the WWFCS targets from which they are defined, are described in Table 1. While these regions are defined according to the WWFCS cluster target locations, we emphasize that these WWFCS targets are not inherently unique, and they form an unbiased subsample of a complete parent cluster sample. Therefore, these WWFCS targets are not treated any differently to other groups and clusters introduced in the subsequent analysis and are used only in the selection of the location of the galaxy sample we analyse.

We find that individual results of each region are comparable and statistically compatible with each other. Moving forward, we therefore opt to stack the galaxy samples of all three regions to enhance our overall statistics. This results in an initial sample of 32 975 galaxies.

2.2 Group and cluster membership

To classify galaxies as members of groups and clusters, we adopt the SDSS DR7 galaxy group catalogue of Yang et al. (2007, hereafter

YGC). This is a catalogue of groups produced from applying an iterative halo-based group finder to the New York University Value added Catalogue (Blanton et al. 2005). The YGC catalogue uses a friend-of-friends algorithm to identify tentative groups, and makes estimates of halo mass, size, and velocity dispersion. These estimates are used to update the group membership, and the estimates are then redetermined. The process is repeated until there is no further change in membership. In this work, we use the halo mass estimate based on ranking group luminosity, as provided by the YGC. In what follows, we define a simple cut-off, and call ‘groups’ those systems from the YGC with halo masses $10^{13}M_{\odot} < M_h < 10^{14}M_{\odot}$, and ‘clusters’ the systems with $M_h > 10^{14}M_{\odot}$.

In this work, we consider only groups with central redshifts contained within the redshift range of each of the regions described in Table 1. In addition, we must also consider the effect of groups and clusters just outside these boundaries. This is because the redshift distributions of galaxies within groups and clusters are elongated along the line of sight due to the Fingers-of-God effect (Jackson 1972). This elongation could bring many of the galaxies residing in groups and clusters whose redshifts are just outside the region boundaries into the redshift bounds. In other words, these galaxies likely have cosmological distances that place them outside the desired range but extend inside because of the Fingers-of-God effect. We therefore choose to remove them to avoid introducing erroneous structures. To identify these galaxy interlopers, we select all groups/clusters whose redshift is at most $2z_{\sigma}$ outside the redshift bounds, where z_{σ} is the velocity dispersion of the group/cluster in redshift units. We then assign galaxies to these groups/clusters if they reside within R_{180} projected distance of a group centre or $2.5R_{180}$ projected distance of a cluster centre (we justify this choice in Section 3.4.4) and if they satisfy $|z - z_{\text{group/cluster}}| < 2z_{\sigma}$. These galaxies likely have cosmological redshifts outside the desired range but have observed redshifts inside due to the peculiar motion induced by their host group/cluster. These galaxies may be misclassified as field or filament galaxies, rather than members of groups or clusters, and must be removed from our sample. Of the 32 975 galaxies in our initial sample, this process removes 852 (2.6 per cent) galaxies, leaving 32 123 galaxies in our sample.

2.3 Masses and star formation rates

We use stellar masses and star formation rates provided by the MPA–JHU catalogue and are retrieved as the quantities `lgm_tot_p50` and `sfr_tot_p50` in the SDSS table `galSpecExtra`. Masses were estimated following the methodology outlined in Kauffmann et al. (2003). Star formation rates were calculated in accordance with Brinchmann et al. (2004) and aperture corrected as described by Salim et al. (2007). Within the regions considered here, of the total 32 123 galaxies, 100 per cent have stellar mass estimates and 32 016 (99.7 per cent) have star formation rate estimates.

The SDSS Main Galaxy Sample is a magnitude-limited sample ($r_{\text{petro}} < 17.77$; Strauss et al. 2002), leading to an increasing mass limit with redshift. To allow comparisons across redshifts, we construct a mass-limited sample. This is done by taking all galaxies within the main galaxy sample and constructing equi-populated bins in redshift containing 5000 galaxies. For each bin, we determine the 90th percentile stellar mass. Applying a logarithmic fit of the form $\log_{10}(M_{\text{stellar}}/M_{\odot}) = A + B \log_{10}(z)$ to these percentiles over the redshift range considered here yields a 90 per cent completeness limit $M_{\text{stellar}} = 10^{9.91}M_{\odot}$ at $z = 0.077$, the largest redshift considered in this work. We retain only galaxies with a stellar mass exceeding this, leaving a total of 23 441 galaxies in our mass-limited sample.

2.4 T-types

To extend this investigation to morphologies, we use the catalogue provided by Domínguez Sánchez et al. (2018), which provides estimates of the galaxy morphologies through the T-Type metric (de Vaucouleurs 1963) for galaxies in the region we consider. These classifications are the result of applying deep-learning models trained on 10 000 T-Type morphological classifications in Nair & Abraham (2010) to 670 722 SDSS galaxies. In contrast to traditional T-Types, these are not restricted to integers. In this scheme, $T\text{-Type} < 0$ corresponds to early-type morphologies (e.g. E, S0) and $T\text{-Types} > 0$ correspond to late-type morphologies (e.g. Sa and later). Of the 23 441 galaxies in our mass-limited sample, 23 026 (98.2 per cent) have T-Type estimates.

3 METHODOLOGY

3.1 Star formation suppression

To isolate the effect of the environment on the star formation activity of the galaxies, we must first account for the variation in star formation rate with stellar mass. To do this, we employ a metric that measures ‘star formation suppression’, ΔSFMS . This is defined as the vertical logarithmic distance to the Main Sequence of star-forming galaxies in the star formation rate versus stellar mass diagram. We identify the Main Sequence, Blue Cloud (BC), and Green Valley (GV) regions by following the work of Trussler et al. (2020):

$$\log(\text{SFR}) = 0.7 \log(M_{\text{stellar}}/M_{\odot}) + b, \quad (1)$$

where b takes values of -7.52 and -8.02 for the BC/GV and the GV/RS boundary, respectively. To define the main sequence of star formation, we adopt the value of $b = -7$, as used in Sampaio et al. (2022). A positive value indicates an enhancement in star formation and a negative value indicates a suppression with respect to star-forming galaxies on the main sequence. We show the star formation rates as a function of stellar mass in Fig. 1 for the whole galaxy sample, indicating the mass-completeness limit as well as the quantity ΔSFMS . This metric of star formation, or similar methods of selecting galaxies based on the distance to the main sequence of star formation, has been used successfully in past studies (e.g. Trussler et al. 2020; Sampaio et al. 2022; Szpila et al. 2024). In Fig. 1, we highlight three identifiable regions, the blue cloud (BC; $\Delta\text{SFMS} > -0.52$) containing star-forming galaxies, the red sequence (RS; $\Delta\text{SFMS} < -1.02$) comprised of quiescent galaxies, as well as the green valley (GV; $-1.02 < \Delta\text{SFMS} < -0.52$), containing galaxies transitioning from the BC to the RS.²

3.2 Local densities

To investigate effects that may impact galaxy evolution on smaller spatial scales, we employ the projected local galaxy density index $\Sigma_3^* = M_3/\pi R_3^2$, with R_3 defined as the distance to the third nearest galaxy neighbour, following Muldrew et al. (2012). To probe the local environment, we use mass density, with M_3 defined as the enclosed stellar mass in a circle of radius R_3 . This definition is comparable to the frequently used number density in system with galaxies of similar mass. It has been shown in the work of Wolf et al. (2009) that number density depends strongly on the selection of the sample,

²The results of this work are unaffected by the exclusion of galaxies with optical signatures of AGNs identified through the BPT classifications provided by the MPA–JHU catalogue, outlined in Brinchmann et al. (2004).

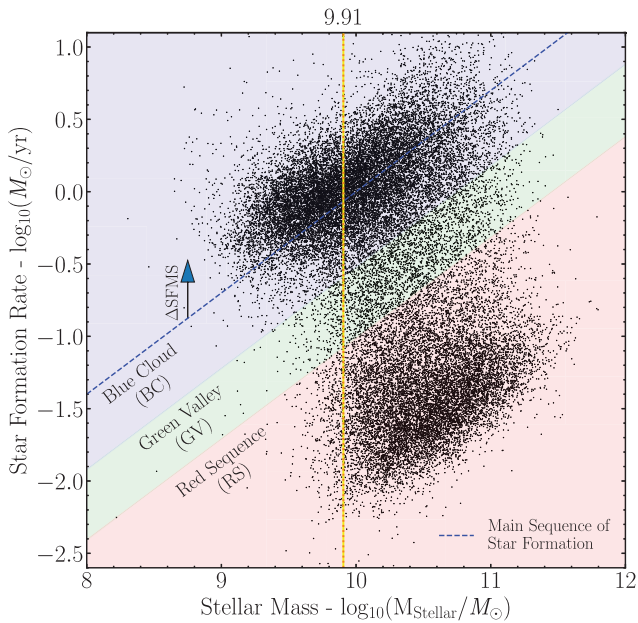


Figure 1. Star formation rate as a function of stellar mass for the galaxies considered in this work. We denote the 90 percent completeness limit at $z = 0.077$ with the yellow vertical dashed line. Shaded in blue is the BC, in green is the GV, and in red is the RS. The dashed blue line denotes the main sequence of star-forming galaxies, calculated using equation (1) with $b = -7$. An illustrative arrow describes the metric of star formation suppression ΔSFMS , used throughout this work. See text for details.

whereas mass density is much more robust to differences in the sample definition.

For galaxies at the edge of the regions, R_3 may overflow past the region bounds, leading to their densities being underestimated. We identify 787 (3.4 per cent) galaxies for which this occurs, and they are not included in the subsequent analysis when local densities are required.

These local galaxy density measurements will be affected by projection effects, where galaxies which are separated a large distance in 3D are included in the density calculation. However, given that the local densities are calculated using the third nearest neighbour, R_3 is relatively small (~ 1 Mpc on average) and so we do not expect that projection effects affect our results.

We emphasize that direct comparisons of local galaxy density indices between different studies is difficult as the resulting densities are dependent on both selection effects and the depth of the redshift window of the sample.

3.3 Cosmic web extraction

Galaxy distributions are expected to trace the cosmic web filaments and we therefore use the galaxies in our sample to map them. Tracing filaments using galaxy distributions is well established with many methods existing to do so. For a list and comparison of some different filament finders, we direct the interested reader to Libeskind et al. (2018). A popular method to extract the cosmic web is using DISPERSE (Discrete Persistent Structures Extractor, Sousbie (2011)). This has been successfully applied in past studies to extract filaments in both 2D and 3D (e.g. Kraljic et al. 2018; Luber et al. 2019; Sarron et al. 2019; Barsanti et al. 2023; Hasan et al. 2023; Bulichi et al. 2024; Galárraga-Espinosa et al. 2024) and it is the tool we use to identify the filament network in this work.

In our case, we use DISPERSE to identify filaments from the Delaunay tessellation of the given galaxy distribution. The persistent topological features (the critical points maxima, minima, and saddle points) of the density field are then identified and filaments are defined as the spatial lines connecting pairs of critical points, i.e. saddle points to the maxima of the density field. A key advantage of using DISPERSE is that it is naturally scale- and parameter-free, while allowing for the selection of only the most robust topological features through the persistence ratio. The persistence ratio quantifies the significance of critical point pairs and can be used akin to a signal-to-noise ratio, removing non-physical features from the filament network.

The choice of persistence ratio is therefore a compromise between the robustness and the number of filaments. A lower persistence ratio adds more weaker, tendril-like filaments to our sample. As we expect that the environmental effect of filaments is subtle, we want to avoid diluting our filament sample with these less significant filaments, thus compromising our ability to detect the possible effects of filaments. Motivated by this reasoning, we adopt a persistence ratio of 2.5 as this allows us to select the strongest, most significant filaments, as is evident from visual inspection (Fig. 2). Similar values have been used successfully in previous studies (e.g. Kraljic et al. 2018; Sarron et al. 2019; Cornwell et al. 2022).

We also include a ‘5 times’ smoothing through the `-smooth` keyword in the `skelconvDISPERSE` function. This smooths the network by averaging each point with the coordinates of its neighbour. This is largely an aesthetic choice and does not affect the results of this work.

With these choices, we are confident to select the dominant filaments responsible for the bulk of galaxy accretion into clusters and therefore relevant for studying pre-processing.

We use the projected 2D distribution of galaxies to extract filaments. This is because at the redshifts considered in this analysis, $\Delta z = 0.02$ corresponds to ~ 5600 km s $^{-1}$ in velocity. The velocity dispersion of a typical galaxy cluster constitutes a sizeable portion of the box depth. Using redshifts as a measure of radial distance could introduce non-physical spurious filaments tracing the distortions of the Fingers-of-God effect. We refer to the work of Kuchner et al. (2021a), which concludes that a 3D cosmic web extraction does not produce reliable filaments in the outskirts of clusters. As a drawback, our choices mean that filaments in this work are largely restricted to those orientated along the plane of the sky. Furthermore, using 2D galaxy positions as tracers for filaments inevitably introduces projection effects. Coherent projection effects result from 3D structures orientated along the line of sight. Structures such as walls viewed edge-on would be indistinguishable from filaments; similarly, filaments viewed end-on could resemble clusters. Spurious projection effects are largely random and the result of contamination from foreground and background galaxies. Given that this contamination is expected to be random, and that DISPERSE is relatively robust to noise, the resulting filament network should be largely unaffected.

We further need to consider unwanted effects introduced close to the edges of our sample area. DISPERSE filaments are subject to edge effects, in the form of spurious filaments tracing the data boundary. A solution would be to extract filaments using the entire main galaxy sample footprint, and then to trim the network to the desired areas of our A, B, and C regions. Region C, however, resides very close to the edge of the footprint and so an alternative approach is required. One solution is that outlined in Cornwell et al. (2022), which involves padding the sample boundary with a random distribution of tracers, with number density equal to that of the sample. We determine this number density using only galaxies further than $2.5R_{180}$ from a cluster centre or R_{180} from a group centre (see Section 3.4). To

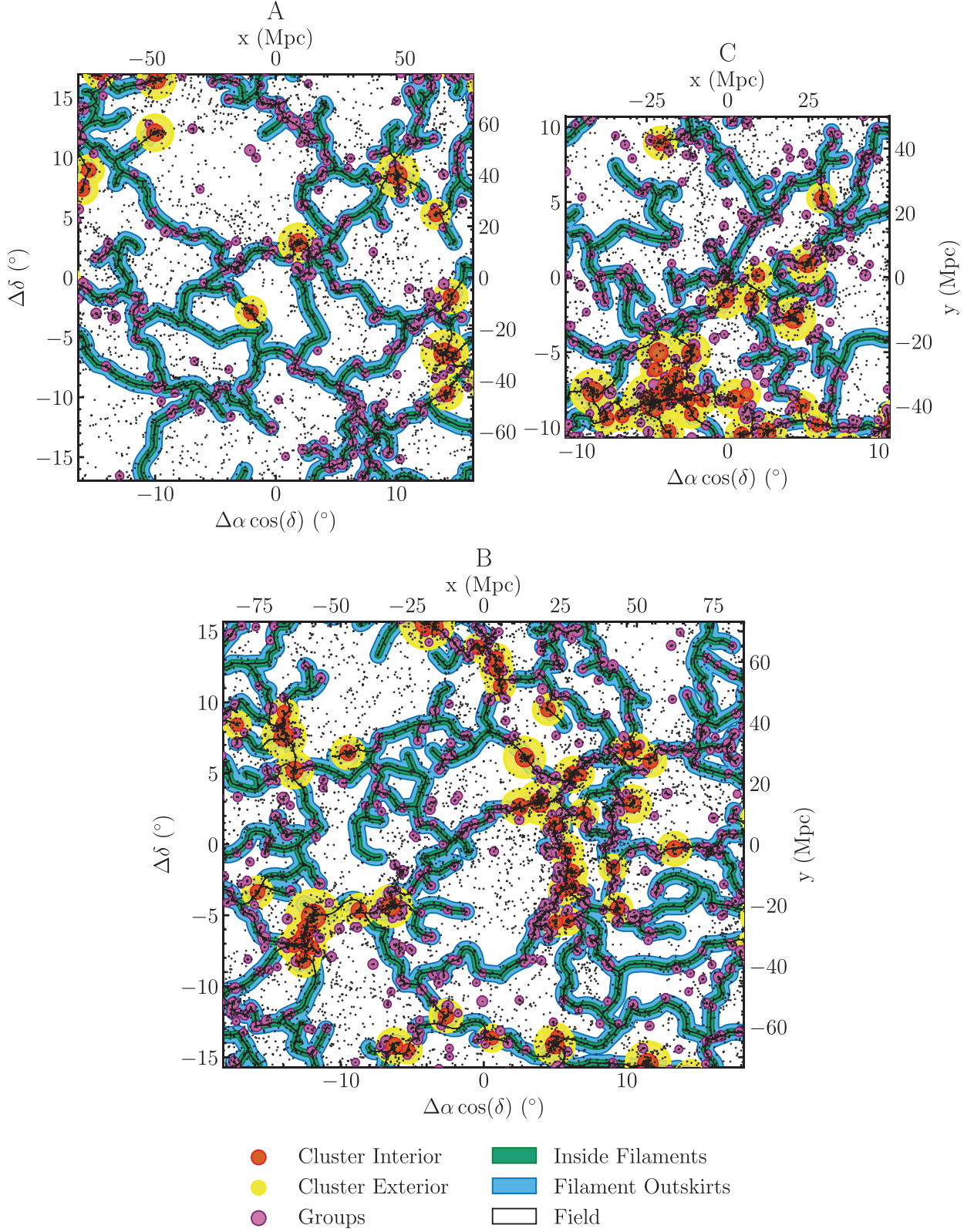


Figure 2. The spatial distribution of galaxies in the mass complete sample considered in this work. Galaxies are shown as black points with DISPERSE filaments as black lines. We identify six distinct environments (see Table 2): Cluster interiors are represented as red circles with radius R_{180} atop yellow circles of radius $2.5R_{180}$, representing cluster exteriors. Groups are displayed as purple circles with radius R_{180} . The surface corresponding to filament membership ($D_{\text{fil}} \leq 1$ Mpc) is shaded in green. Filament outskirts are similarly shaded in blue, covering the area out to $D_{\text{fil}} = 2.5$ Mpc.

determine whether this approach is valid, we compare both methods for regions A and B, and find that they produce very similar filament networks.

3.4 Classifications for galaxy environments

In this section, we detail the identification of galaxies belonging to any of the six environmental classes highlighted in Fig. 2.

3.4.1 Inside filaments

We classify galaxies as members of filaments using the smallest projected distance to a filament D_{fil} . We calculate physical projected distances using the angular diameter distance of the central redshift of the region z_{centre} .³

We model filaments using the skeleton file output of DISPERSE. This provides a list of segments that make up the filament network. Segments are considered to be linear in angular coordinates ($\Delta\alpha \cos \delta$, $\Delta\delta$), with $\Delta\alpha = \alpha - \alpha_{\text{centre}}$ and $\Delta\delta = \delta - \delta_{\text{centre}}$. From this, filaments are modelled as a continuous structure, allowing distances to be determined to any point on the filament.

Past studies have generally found that filaments possess a characteristic radius of the order of ~ 1 Mpc (Colberg, Krughoff & Connolly 2005; Aragón-Calvo et al. 2010; Bond, Strauss & Cen 2010; Gonzalez & Padilla 2010; Cautun et al. 2014; Kuchner et al. 2020; Castignani et al. 2022a; Wang et al. 2024). We opt to classify galaxies as members of filaments if they reside within 1 Mpc projected distance of a filament. In this scheme, filaments are treated as a homogeneous set with a constant radius. This is an approximation for physical filaments, with their radius and other properties such as density varying as a function of distance to clusters (Pimblet, Drinkwater & Hawkrigg 2004; Gonzalez & Padilla 2010; Cautun et al. 2014; Kim et al. 2016; Wang et al. 2024). Nevertheless, an approximately constant radius is sufficient for our purposes, and a more sophisticated treatment is not necessary given other uncertainties.

3.4.2 Filament outskirts

Filaments are high-vorticity structures, with both gas and dark matter profiles known to be well described by a self-gravitating isothermal profile (Ramsøy et al. 2021; Lu et al. 2024). There is, however, evidence to suggest that filaments are also highly complex. One such example is the one presented by Lu et al. (2024), which investigates the radial profile of three simulated Mpc-scale filaments at $z \sim 4$. They found that the radial profile of filaments can be described with three zones: an inner zone with cold dense gas, an intermediary zone dominated by vortices due to inflowing and post-shock gas, and an outer zone where outwards thermal pressure decelerates inflowing gas. While the structure of filaments at $z \sim 0$ is currently not well understood, Song et al. (2021) provide evidence that at $z \sim 2$, the distribution of haloes around filaments is bimodal, with some galaxies very close to filaments and others further away (~ 1 Mpc). The authors find that the efficiency of galaxy mass assembly is specific to the distance to a filament spine, with galaxies at the edge of

³Throughout this analysis, we determine projected distances using the small triangle approximation. Over the areas considered in this work, this leads to at most a ~ 8 per cent error over ~ 100 Mpc scales relative to the exact treatment. Given its simplicity and computational advantage, we decided to use this approximation since none of our results are affected.

filaments potentially subject to unique quenching mechanisms. This suggests that a simple description of filament membership or not is insufficient and motivates the inclusion of a secondary filament environment, the filament outskirts. This environment further aids our investigation by increasing the contrast between the filament and field populations, allowing for a ‘buffer zone’ separating ‘true’ filament galaxies from field galaxies that are most likely not to have interacted with the higher density regions of the cosmic web. We classify galaxies as members of filament outskirts if they satisfy $1\text{Mpc} < D_{\text{fil}} < 2.5\text{Mpc}$.

3.4.3 Field

Galaxies in the field form our control sample. These are galaxies which exist in low-density regions and are unlikely to be influenced by collapsed elements of the cosmic web, e.g. walls, filaments, and nodes. We classify galaxies as members of the field if they satisfy $D_{\text{fil}} > 2.5\text{Mpc}$ and are not members of higher density environments such as groups, clusters, and their outskirts (see later).

3.4.4 Cluster and groups

Galaxies which have been affected by the cluster and group environments must be removed from our sample of filament members if we are to isolate the effect of the filament environment itself. These galaxies may have already undergone some transformation, which could erroneously be interpreted as the effect of filaments if they are not removed from the filament galaxy sample. This exclusion is commonplace in the literature; one example is presented in the work of Laigle et al. (2018), in which galaxies closer than some distance to a cluster/group are excluded from the sample. We adopt a similar approach. We use the R_{180} estimates provided for groups and clusters in the YGC, where R_{180} is the radius of a sphere whose mean density is 180 times the critical density. We determine R_{180} using equation (5) in Yang et al. (2007).⁴

We classify galaxies as members of clusters/groups using the projected distances to a cluster/group centre, in combination with the velocity dispersion of the cluster/group. We determine the line-of-sight velocity dispersion using equation (6) in Yang et al. (2007). Galaxies within projected R_{180} of a cluster/group centre, and with redshifts such that $|z - z_{\text{cluster/group}}| < 3z_{\sigma}$, are classed as members of the group/cluster interiors. These classifications of group and cluster interior galaxies are similar to what is often referred as ‘cluster members’ and ‘group members’ in previous works. We note that the results presented in this paper do not change if we assign memberships entirely in 2D, defining cluster/group members as those galaxies inside a cylinder of radius R_{180} and height $\Delta z = 0.02$.

For galaxies within this projected distance, but with redshift exceeding $\pm 3z_{\sigma}$, it is not clear what environment these belong to. As such, of the 23 441 galaxies in our sample, 1387 (5.9 per cent) galaxies are not given any classification and are not considered in the following analysis comparing galaxies in different environments.

This treatment is not sufficient to remove the influence of clusters due to the existence of ‘backsplash’ galaxies. These are defined in the literature as galaxies which have been within R_{200} of a cluster at some point in the past but are now located further away (Gill,

⁴ R_{180} is somewhat larger than the commonly used R_{200} , and therefore provides a more conservative exclusion zone around clusters and groups. Moreover, since the YGC provides R_{180} directly, we prefer to use this value rather R_{200} to avoid model-depending scaling.

Table 2. Summary of the environmental classification scheme and the ranking of the six distinct environments (see Fig. 2). Galaxies which satisfy multiple classifications are assigned the environment with the highest rank (see Section 3.5).

Ranking	Environmental classification	N
6	Cluster interior: $<R_{180, \text{cluster}}$	3105 (13.2%)
5	Group: $<R_{180, \text{group}}$	4110 (17.5%)
4	Cluster exterior: $<2.5R_{180, \text{cluster}}$	1765 (7.5%)
3	Inside filaments: $D_{\text{fil}} < 1\text{Mpc}$	4905 (20.9%)
2	Filament outskirts: $D_{\text{fil}} < 2.5\text{Mpc}$	2918 (12.4%)
1	Field: $D_{\text{fil}} > 2.5\text{Mpc}$	5251 (22.4%)
N/A	Unclassified	1387 (5.9%)

Knebe & Gibson 2005; Bahe et al. 2013). Using observational data it is not possible to definitively identify individual backplash galaxies; only the probability that a galaxy is backplash can be determined. Kuchner et al. (2021b) found that, for clusters, at R_{200} 30–60 per cent of galaxies within filaments are likely to be backplash, with the exact number dependent on the cluster dynamical state. This probability vanishes at $\sim 2.5R_{200}$. To account for these backplash galaxies, we classify galaxies as members of the ‘cluster outskirts’ if they are within R_{180} and $2.5R_{180}$ of a cluster centre. Note that we still use R_{180} in this work as a slightly larger and therefore more conservative estimate of the clusters’ sphere of influence than R_{200} .

Backplash galaxies in groups are expected to be fewer than those of clusters, resulting from their reduced richness and gravitational potential. As a result, we do not attempt to correct for backplash galaxies in groups. Furthermore, since groups are overwhelmingly located in filaments, removing galaxies within $2.5R_{180}$ of groups unnecessarily decreases our filament galaxy sample.

3.5 Environmental overlaps

Many galaxies in our sample satisfy more than one of the classification criteria. We therefore assign a hierarchy of classifications, to prevent overlaps. When assigning a galaxy to an environmental class, if it meets the criteria for more than one class, it is allocated to the class with the higher rank (‘denser’ environment). This ranking is presented in Table 2. This is to avoid mixing high- and medium-density environments in an attempt to separate their associated environmental effects (for a detailed discussion of the environmental effects in high-density environments, particularly the difference between those in clusters and groups, we direct the interested reader to the recent review of Alberts & Noble 2022). It is shown in table 4 of Aragón-Calvo et al. (2010) that different components of the cosmic web possess a characteristic density, with clusters denser than filaments, which are in turn more dense than voids. We expect that clusters should be of a higher density than groups, due to their increased richness and halo mass. Using the reasoning above, the cluster outskirts must be ranked higher than filaments to account for backplash galaxies. Galaxies often fall on to clusters as part of groups, therefore we opt to rank groups higher than the cluster outskirts to retain these infalling groups as part of the group class.

4 RESULTS AND DISCUSSION

In this section, we first compare the cumulative distributions of galaxy properties within each environment. We then repeat the analysis but accounting for differences in stellar mass distributions across environments by matching the galaxy samples in mass. Finally, we account for differences in the local galaxy density distributions and

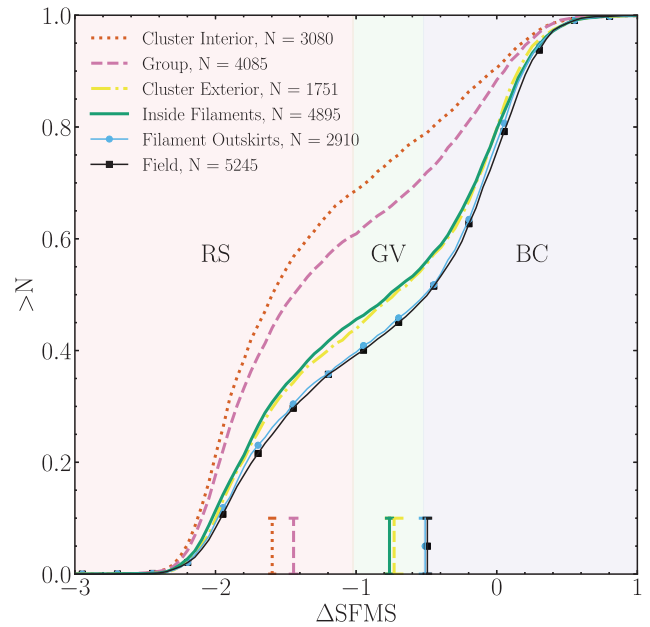


Figure 3. The cumulative distributions of star formation suppression ΔSFMS for the galaxies in each environment. Medians of each distribution are shown as vertical lines along with their respective 1σ errors. Shaded in red is the region corresponding to the RS, in green is the GV, and in blue is the BC. The numbers of galaxies in each environmental bin are shown in the legend. It is clear from the cumulative distributions that galaxies inside filaments tend to be suppressed in star formation relative to those in the field, while galaxies in groups and cluster interiors tend to be suppressed in star formation relative to those in filaments. This suggests that filaments may act as an intermediary environment.

present the results obtained with samples matched in both stellar mass and local galaxy density. We present the results for the star formation suppression index ΔSFMS in Section 4.1 first and for the galaxy morphologies in Section 4.2.

4.1 Star formation suppression

4.1.1 Full galaxy samples

Galaxies in groups and clusters have suppressed star formation compared to those in filament galaxies, which are in turn more suppressed than field galaxies (Fig. 3). This is evident from their cumulative distributions of ΔSFMS . While this immediately suggests the presence of environmental effects and, in particular, pre-processing in filaments, there is strong evidence that stellar mass is a key factor driving the properties of galaxies (e.g. Oesch et al. 2010; Alpaslan et al. 2015). As such, to ensure that the effects observed are truly a consequence of the environment and not due to differences in mass, we need to compare the stellar mass distributions between the galaxy populations across environments.

4.1.2 Stellar mass distribution

To ascertain the effects of stellar mass on the observed trends in ΔSFMS , we investigate how the stellar mass functions are correlated with the environment. For the galaxies in each environmental class, we present the cumulative mass distributions in Fig. 4. It is clear that the distributions are not equal. Cluster interiors and groups tend to be significantly more massive than those in filaments. We also

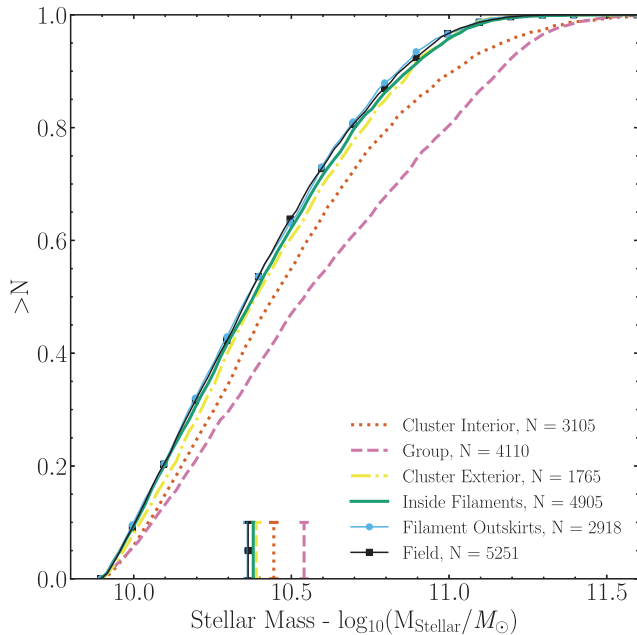


Figure 4. The cumulative distributions of galaxy stellar mass for the galaxy populations in each environmental bin. Medians for each distribution are shown by vertical lines along with their respective 1σ errors. The numbers of galaxies in each environment are shown in the legend. It is clear that ‘denser’ environments tend to possess galaxies with higher stellar masses. Curiously, we find that galaxies in groups tend to be of higher masses than those in cluster interiors, a trend which is discussed in Section 4.1.2.

find hints of a difference between the stellar mass distributions of galaxies in filaments and those in the field, this difference is small and statistically insignificant ($p = 0.149$).

Galaxies near filaments tending to be more massive than those further away is a well-established result in the literature. Mass gradients have been reported in many prior studies, examples include Alpaslan et al. (2015), Malavasi et al. (2017), Ricciardelli et al. (2017), Kraljic et al. (2018), Sarron et al. (2019), Song et al. (2021), Bulichi et al. (2024), and Hoosain et al. (2024). This trend can be explained by an enhancement of merger rates inside filaments (Malavasi et al. 2017). Alternatively, this could be the result of the biasing of the mass function around the LSS (Kaiser Bias; Kaiser 1984), who propose that the enhanced density field facilitates an earlier collapse of proto-haloes, leading to an excess of massive galaxies in denser environments.

Surprisingly, we find that galaxies in groups tend to be of higher masses than galaxies in clusters. The effect is small, with the median stellar mass 0.1 dex (26 per cent) higher in groups than in cluster interiors (a 6.75σ difference). This result contradicts that of Alpaslan et al. (2015), who investigated how the galaxy stellar mass functions vary as a function of cosmic web environment using GAMA data. Their galaxy stellar mass functions for high- and mid-mass groups correspond to those of our clusters and groups, respectively. Contrary to our findings, Alpaslan et al. find that their high-mass groups (corresponding to our clusters) generally contain a larger proportion of high-mass galaxies than their mid-mass groups (what we call ‘group’). We do not have a clear explanation for this contradiction but, given the relatively small size of the effect and the differences in sample selection and mass determination, it is perhaps not too surprising that our results do not match exactly.

It is nevertheless clear that differences in the stellar mass distributions may be responsible for the trends observed in Fig. 3. To account for this, we will construct mass-matched samples (i.e. samples with identical stellar mass distributions).

4.1.3 Δ SFMS–mass matched sample

We construct mass-matched samples through pairwise comparisons of each environment. We construct these mass-matched samples as follows. For each environment pair (e.g. inside filaments and field), we take each galaxy within the class with the smallest number of galaxies, and find its pair in the other with the closest mass. If this mass is within 0.1 dex, then both galaxies are added to their respective mass-matched samples. In this procedure, we do not allow for replacement.

We present the results of this pairwise comparison in Fig. 5. We find that the trends shown in Fig. 3 are also evident in the mass-matched pairwise comparisons. We find that when mass-matched, galaxies inside filaments tend to be suppressed in star formation relative to the field population and further suppressed relative to galaxies in groups and within the interiors of clusters. This supports the argument that filaments may be an intermediary environment, between the field and clusters.

Interestingly, we find that the Δ SFMS distributions for filaments and cluster outskirts are similar (both for the mass-matched samples and the un-matched ones). In hindsight, this should not be surprising – based on simulations, Kuchner et al. (2021b) show that the outskirts of clusters are highly heterogeneous environments, with up to 45 per cent of galaxies in this region closer than $1h^{-1}$ Mpc to a filament spine, with 28–58 per cent (dependent on cluster dynamic state) unaffected by the cluster. As such, the population of the cluster outskirts is expected to consist mainly of filament, and field galaxies and therefore it is expected that galaxies in the cluster outskirts show little difference from the filament and field populations.

The increased star formation suppression within filaments, in comparison with the field, agrees with the results of past studies such as Martínez et al. (2016), Kraljic et al. (2018), and Laigle et al. (2018), as well as simulation work (e.g. Bulichi et al. 2024). The increased passive fraction and suppressed star formation of filament galaxies relative to the field can be interpreted as galaxies undergoing some degree of pre-processing inside filaments before they infall into clusters.

The analysis of the effect of filaments on star formation with mass-matched samples is commonplace in the literature. However, while this indicates that the filamentary environment does indeed play a role in shaping galaxy properties, it is not clear if these differences in Δ SFMS are driven by the physical processes associated with the small-scale or the large-scale environment. By parametrizing the local environment of a galaxy through the local galaxy density index Σ_3^* (Fig. 6), we attempt to gain insight into this by constructing samples matched in both stellar mass and local galaxy density.

4.1.4 Δ SFMS–mass and local-density matched samples

The distributions of Σ_3^* for the different environments are shown in Fig. 6. Although the range of densities present in each environment is quite diverse, there is enough overlap to build density-matched galaxy samples for all pairs of environments.

Following on what we did before, we now carry out pairwise comparisons between each environmental bin with samples matched

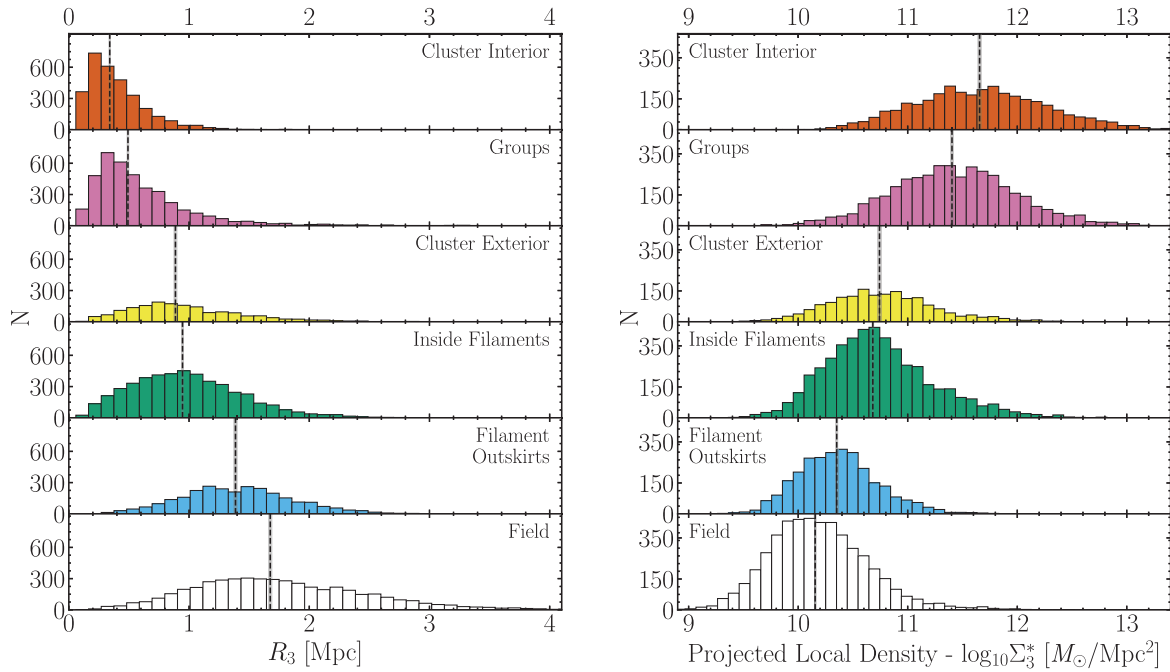


Figure 6. (Left column) Distributions of the distance to the third nearest neighbour R_3 . (Right column) Distributions of the projected local galaxy density index Σ_3^* . Each panel corresponds to a separate environmental class, coloured consistent with the other figures in this work. Medians of each of the distributions are shown by vertical dashed lines as well as the 1σ errors shown by the shaded grey area. The environments considered in this work possess different, yet overlapping R_3 and local density distributions, highlighting both the multiscale nature of the cosmic web and the need to consider both the local and large-scale environment. The median value of R_3 in filaments is ~ 1 Mpc, half the width of the filaments considered in this work. This shows that R_3 is an ideal choice to probe the internal environment of filaments as it tends to probe the density inside filaments themselves. This is also the case for other environments such as groups and cluster interiors – R_3 measures densities *inside* each specific environment.

While it is not possible to conclude what these processes are with the available information, we can speculate what these could be. One natural choice is an enhanced rate of galaxy–galaxy interactions; this environmental effect will be elevated inside filaments due to the increased number density of galaxies relative to the field. Local galaxy density acts as a proxy for such effects and could explain the differences seen between the mass-matched samples, but not seen in the mass- and local galaxy density-matched ones. This scenario would be consistent with the results and previous works discussed in Section 4.1.2 which find that filament galaxies tend to have a greater stellar mass compared to those in the field, perhaps hinting at an enhanced merger rate inside filaments.

Additionally, while the difference observed in the mass-matched samples may be due to environmental processes governed by local galaxy density, it could also be that the relevant physics simply *correlates* with it. One such possibility could be that the differences are a consequence of elevated galaxy halo masses at fixed stellar masses. Oyarzun et al. (2023) find that galaxy halo mass is an important parameter in describing the properties of passive satellite galaxies. Similar results are found by Scholz-Díaz, Martín-Navarro & Falcón-Barroso (2022) for central galaxies and by Zhou, Aragón-Salamanca & Merrifield (2024) for central disc galaxies. Simulations such as those of Wang, Wang & Chen (2023) also point towards the importance of halo mass in driving galaxy evolution, even at fixed stellar mass. There is evidence that galaxy halo mass is correlated with stellar mass (Wu, Jespersen & Wechsler 2024) and local density (Haas, Schaye & Jeon-Daniel 2012; Muldrew et al. 2012). While the extent of the correlation between galaxy halo mass and local density is disputed, especially for low galaxy halo masses ($\log(M/M_\odot) < 13$), it is possible that the differences seen in Fig. 5

could be due to the difference in galaxy halo mass distributions in the stellar mass-matched samples across environments. It is too early to pinpoint the exact effect these differences in halo masses would have on specific galaxy properties such as Δ SFMS, but there is a growing body of empirical and theoretical evidence suggesting that it may be important.

Another possibility is that these differences are a consequence of ‘archaeological downsizing’ (Thomas et al. 2005). Galaxies residing in overdense regions likely formed before those in underdense regions, with the enhanced density field facilitating an earlier proto-halo collapse. Given that these galaxies will have begun assembling their stellar populations earlier, and mass quenching is strongly mass dependent with higher mass galaxies quenching first (e.g. Popesso et al. 2011; Sobral et al. 2011; Darvish et al. 2016), it is expected that galaxies in dense environments such as clusters, groups, and filaments, should have an excess of older galaxies relative to those in the field. Therefore, it is also possible that the observed suppression in star formation of filament galaxies is at least in part a result of older stellar ages. Given that we do not have age estimates for the galaxies in this work, we cannot investigate the extent to which differing ages could contribute to these observed differences.

While most of the differences in the Δ SFMS distributions across environments disappear when we match both in stellar mass and local galaxy density, some significant differences persist—albeit at a small level—when comparing other environments with cluster interiors. This suggests that even if part of the environmental effect of cluster interiors can be characterized by local galaxy density, there are additional physical processes not directly correlated with it. This means that, in many ways, these are unique environments where galaxies are subject to physical processes beyond those linked with

Mass and Density Matched

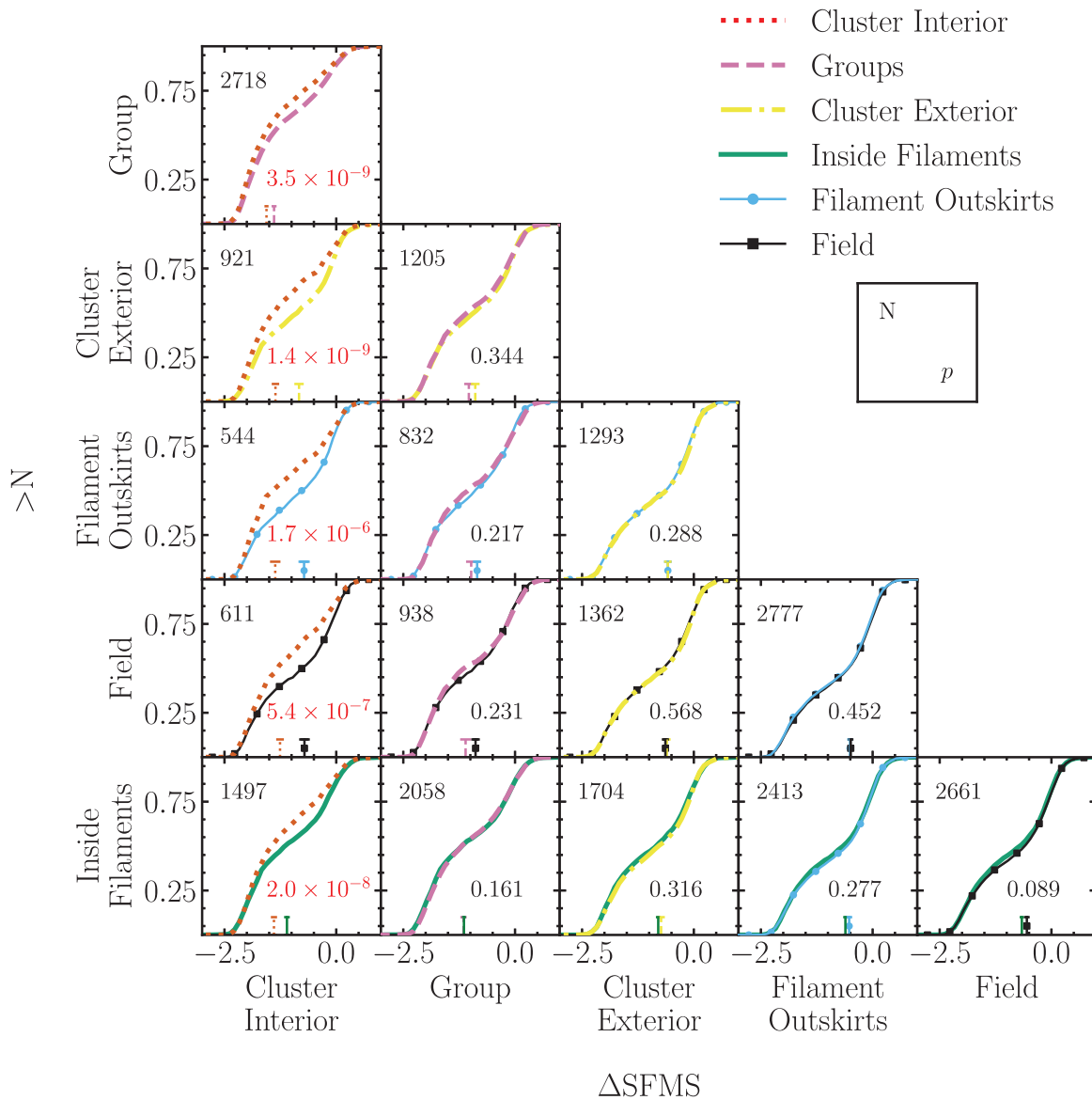


Figure 7. Pairwise comparisons of the Δ SFMS distributions for each environmental pair using the mass- and local galaxy density-matched samples. Medians of each distribution are shown as vertical lines with their respective 1σ errors. In each panel, the number of galaxies in each population is shown in the top left. Using Kolmogorov–Smirnov statistics, the probability that both distributions are identical is shown in the lower right. Significant p -values ($p < 0.05$) are coloured in blue and highly significant p -values ($p < 0.01$) are coloured in red. While the differences between the filament population observed in the stellar mass matched samples (Fig. 5) persist between filaments and cluster interiors, the difference between the filament population and the field vanishes. This suggests that the environmental effect on Δ SFMS of galaxies within filaments can entirely be characterized by a local galaxy density index Σ_3^* .

local galaxy density. One candidate is ram-pressure stripping by the ICM. There is strong evidence that galaxies infalling into galaxy clusters show signatures of ram pressure stripping (e.g. Poggianti et al. 2017; Vulcani et al. 2020, 2022). However, whether or not signatures of ram pressure stripping in filaments are to be expected, is not entirely known. In the work of Thompson, Smith & Kraljic (2023), a set of void simulations are used to investigate the ability of haloes to accrete gas in voids, finding that even in low-density void walls, ram pressure stripping can occur, impairing the accretion of gas. Furthermore, Song et al. (2021) find using the HORIZON-

AGN simulations that the high vorticity regions of filament edges could reduce the efficiency of gas transfer within galaxies due to the coherent and large angular momentum of the outer halo as fed by these vorticity rich filaments. The work of Kotecha et al. (2022) using The Three Hundred Project simulations suggests that filaments may even shield galaxies from the ICM and limit ram pressure stripping, with cluster galaxies near filaments tending to be more star-forming than those further away. As discussed in Darvish et al. (2014), ram-pressure stripping is not expected to be an effective mechanism to suppress star formation within filaments due to the reduced density

of the intergalactic medium relative to the ICM, together with the smaller velocities of filament galaxies compared with those inside clusters. Together with the trends shown in Fig. 7, this suggests that clusters may be extreme and unique environments with additional environmental effects not experienced by galaxies in filaments alone.

We again emphasize that given the available information, we can only conclude that Σ_3^* encodes the differences observed in the mass-matched samples of filaments and field. The above discussion concerning the possible mechanisms and physical processes is reasonable and plausible, but speculative. We do not yet have the required information to make firmer conclusions. As we discuss in Section 5, exploring the star-forming histories of galaxies living in different environments will help us to make progress.

We cannot end this discussion concerning galaxy densities without pointing out that the scale at which one computes galaxy density probes environment and the related physics on different spatial scales. Small scales probe the local environment and the most recent and stochastic processes, whereas larger scales take into account the integrated – and thus smoother – environmental history of the galaxies. Moreover, since using $n = 3$ when computing Σ_n^* is somewhat arbitrary, we checked that our results persist for $n = 5$. Finally, even though we argued in Section 3.2 that using $\Sigma_n^* = M_n/\pi R_n^2$ makes more physical sense than using $\Sigma_n = n/\pi R_n^2$ (ignoring the mass of the companion galaxies), we checked that using Σ_3 instead of Σ_3^* leaves our results largely unchanged also.

4.2 T-Types

We now extend our analysis to galaxy morphologies using T-Types. We present the T-Type cumulative distributions for the whole sample in Fig. 8. We observe similar trends as in Δ SFMS (cf. Fig. 3), where the cluster interior and group environments are significantly biased towards earlier type morphologies relative to the other environments. We also find a difference between the filament population and the field, in which filament galaxies preferentially exhibit more early-type morphologies than field ones. This suggests that filaments do contribute, at least to some extent, to the morphological transformation of galaxies. However, as before, we must match our samples in mass before any inferences can be made about the specific effect on the environment.

4.2.1 T-Type–mass matched samples

We present the pairwise comparisons of the mass-matched samples in Fig. 9. We find that there appears to be a small yet statistically significant difference between the T-Type distributions of the filament and field populations ($p = 1.4 \times 10^{-3}$). We find that galaxies in filaments tend to be slightly more early-type in morphology than those in the field, suggesting that galaxies in filaments may be subject to pre-processing not only affecting their star formation but also their morphology.

These results are consistent with an increased elliptical-to-spiral ratio within filaments compared to the field, a result that is well established in the literature (Kuutma et al. 2017; Ricciardelli et al. 2017). The simulation work of Song et al. (2021) suggests that galaxies in the centre of filaments tend to have a more compact stellar distribution, which could be the result of efficient angular-momentum cancellation from filamentary flows. All these results suggest that the filament environment does play a role in shaping the morphology of galaxies. This, however, is not clearly seen in the

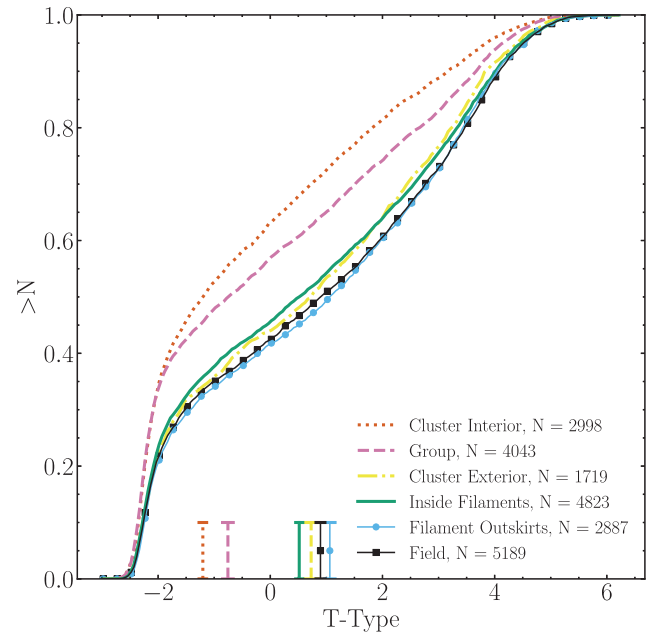


Figure 8. Cumulative distributions of T-Types for the galaxy populations in each environmental bin. Medians of each distribution are shown as vertical lines along with their respective 1σ errors. As with Δ SFMS, we find that galaxies inside filaments tend to favour more early-type morphologies than those in the field, while galaxies in groups and cluster interiors tend to possess more early-type morphologies than those in filaments. This suggests that filaments act as intermediary environments for morphological transformations.

work of Alpaslan et al. (2015), which finds that, after normalization in mass, the morphologies of galaxies in non-group environments (e.g. filaments and voids) are largely similar. However, these authors do find small differences in ellipticity, possibly suggesting that discs may be more likely to be found in voids, in some agreement with our findings.

We find that galaxies in cluster interiors tend to possess the highest fraction of early-type galaxies. Given the local galaxy density distributions shown in Fig. 6, this is not surprising, as highlighted by the morphology–density relation that galaxies in more dense environments favour early-type morphologies. To determine whether or not these differences, as well as those seen in filaments, are a consequence of the processes associated with the large-scale or small-scale environment, we must account for the differences in local galaxy density distributions, as we did before. To accomplish this, we construct samples matched both in stellar mass and local galaxy density.

4.2.2 T-Type–mass and local density-matched samples

We find that the effects of filaments can be entirely encoded within a local galaxy density index. This is evident in Fig. 10, where we repeat the above analysis for samples matched both in stellar mass and local galaxy density. We find that the differences observed between the filament and field populations in the mass-matched samples vanishes when also matching in local galaxy density. This suggests that similarly to Δ SFMS, the differences observed in the mass-matched samples are a consequence of the different local galaxy density distributions between the filament and field sample, as is expected given the morphology–density relation.

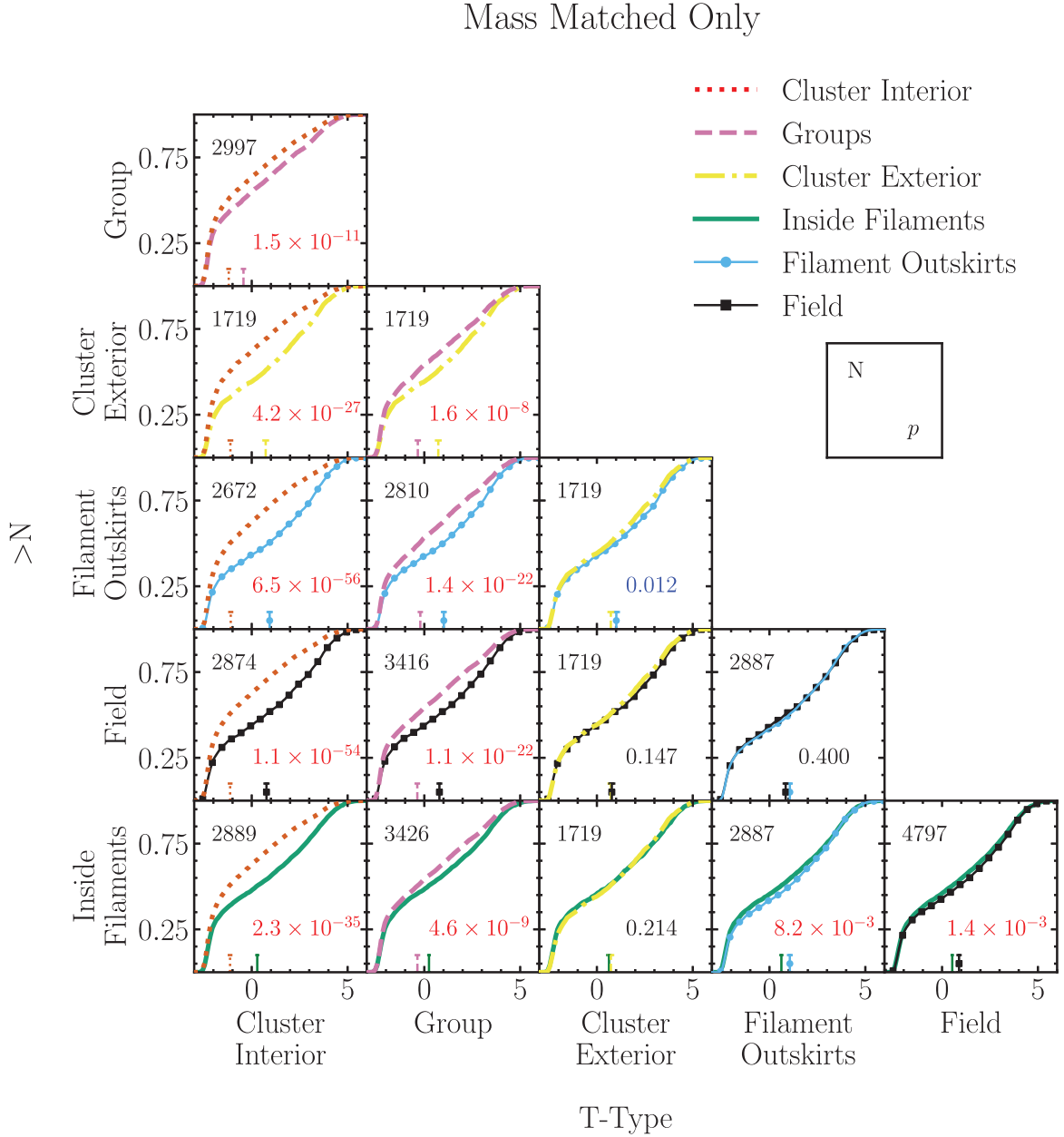


Figure 9. Pairwise comparisons of the T-Type distributions for each environmental bin pair, using the mass-matched samples only. Medians for each distribution are shown as vertical lines along with their respective 1σ errors. In each panel, the number of galaxies in each population is shown in the top left. Using Kolmogorov–Smirnov statistics, the probability that both distributions are identical is shown in the lower right. Significant p -values ($p < 0.05$) are coloured in blue and highly significant p -values ($p < 0.01$) are coloured in red. There are significant differences between the T-Type distributions between the mass-matched samples of galaxies within filaments compared to those in cluster interiors and the field. This suggests that when matching in mass only, filaments act as an intermediate environment between clusters and the field.

This further supports the conclusions discussed in Section 4.1.4, in which the environmental effect of filaments can entirely be characterized by local galaxy density. The interpretation and the discussion presented there of the possible physical mechanisms at play is also valid here.

Similarly to what we found for Δ SFMS, the only differences between the T-Type cumulative distributions can be found when comparing cluster interiors with lower density environments. This suggests that galaxies in the clusters are subject to additional environmental effects affecting their morphology that are not characterized by local galaxy density alone. Gravitational tidal effects due to the

cluster potential is a plausible mechanism for this, in addition to ram-pressure stripping.

Numerous past studies have attempted to account for the effect of local galaxy density in this context; one such is the work of Kuutma et al. (2017), which finds that the elliptical-to-spiral ratio decreases with increasing distance from filaments, after normalizing in both mass and density. We note that this is not necessarily in disagreement with our work, as we opt to identify galaxies within filaments which are also members of groups or clusters and consider them separately, and not as members of the filaments themselves. As such, the trends observed by Kuutma et al. (2017) may be driven by

Mass and Density Matched

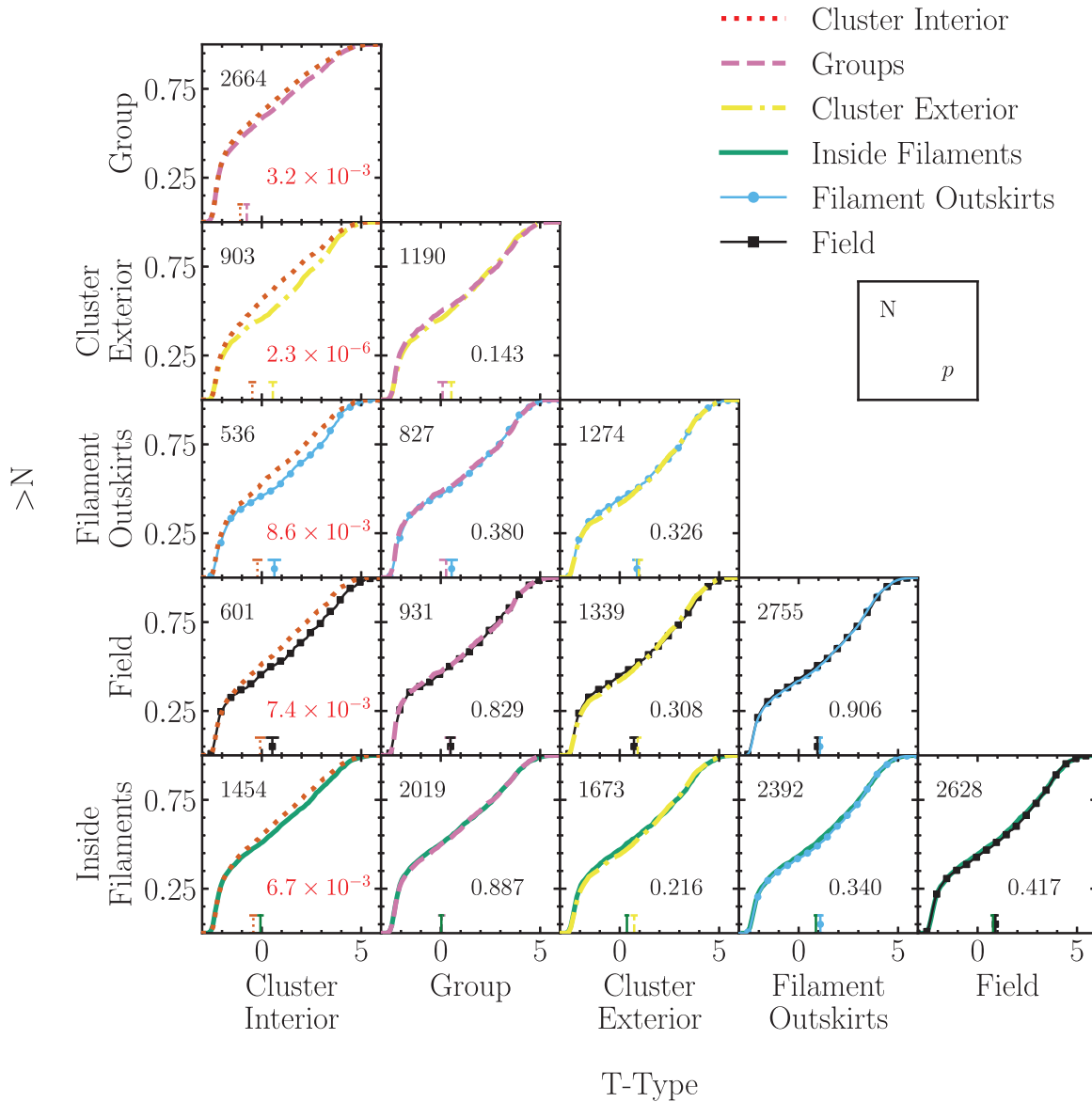


Figure 10. Pairwise comparisons of the T-Type distributions for each environmental bin pair, using the mass- and local density-matched samples. Medians for each distribution are shown as vertical lines along with their respective 1σ errors. In each panel, the number of galaxies in each population is shown in the top left. Using Kolmogorov–Smirnov statistics, the probability that both distributions are identical is shown in the lower right. Significant p -values ($p < 0.05$) are coloured in blue and highly significant p -values ($p < 0.01$) are coloured in red. When matching in local galaxy density also, we find that the difference in the T-Type distributions between the filament and field population seen in the mass-matched comparison (Fig. 10), vanishes. This suggests that the environmental effect of filaments on galaxy T-Type can be entirely parametrized by a local galaxy density index Σ_3^* .

the group and cluster populations within filaments. We further note that this discrepancy may be due to differences in methodologies also, such as different environmental density and filament sample definitions.

Additionally, Castignani et al. (2022a) investigate how galaxy morphology varies in filaments around the Virgo cluster as a function of local galaxy density. The authors conclude that filament galaxies tend to have a decreased late-type fraction compared to the field population. However, these results are at fixed local galaxy density only, without accounting for stellar mass. It has been shown in this

work (Fig. 4) as well as previous works such as Alpaslan et al. (2015) that stellar mass distributions tend to vary between cosmic web environments. It is possible then that the difference seen by Castignani et al. (2022a) could be a consequence of different stellar mass distributions, different methodologies, and/or the result of including lower mass galaxies in their sample given the proximity of the Virgo cluster. We discuss the implications of considering lower mass galaxies than those in this work in Section 4.3.

As we did in Section 4.1, we find that swapping to the local number density index Σ_n does not affect the conclusions of this work. We

do find small changes when going from Σ_3^* to Σ_5^* , we find that the differences between cluster interiors and groups vanishes, while we observe only a small but statistically insignificant ($p = 0.272$) difference between cluster interiors and the field. It is likely the latter is a result of the small overlap in density distributions at this larger scale. The lack of difference between cluster interiors and groups at the larger scale could be a result of the inability to find analogues for the densest, most central of galaxies in groups at this larger scale. This hints that the difference seen between cluster interiors and groups could be driven by galaxies residing in the densest, most central regions of clusters. However, we stress that the main objective is investigating the effects of filaments, the conclusions of which are unchanged with the different local galaxy density indices tested above.

4.3 Pre-processing and the effect of filaments

We consider now what these results mean for pre-processing within filaments. We must emphasize that observational studies, such as this work, are restricted to the present environment only, while this does indeed correlate with the historic environment, it does not fully describe it. We must therefore be cautious in allocating the effects of the current and observed environment, which actually may be a result of the past environment.

In Figs 3 and 8, we find that galaxies in filaments tend to be suppressed in star formation and favour earlier type morphologies relative to the field population. We further show that this effect persists when matching in stellar mass in Figs 5 and 9. This suggests that galaxies in filaments could be subject to environmental effects and that filaments of the cosmic web serve as important intermediate environments for galaxy evolution.

We find, however, in Figs 7 and 10 that when matching also in local galaxy density, the differences between the filament and field populations vanish. We conclude that the effects of filaments can be entirely encoded within a local galaxy density index, suggesting that the effects within the mass-matched sample are a consequence of the star formation–density and morphology–density relations due to the differing local galaxy density distributions. We find no evidence suggesting that filaments impart unique environmental effects that cannot be characterized by local galaxy density. While this conclusion holds for the galaxy sample considered in this work, we note that our conclusions on the role of filaments are subject to our mass limit ($M_{\text{stellar}} > 10^{9.91} M_{\odot}$). Given that low-mass galaxies are affected more strongly by mechanisms present in higher density regions of the cosmic web, this is important to consider.

The efficiency of many environmental processes is dependent on the mass of the galaxy on which they act. One such example is ram-pressure stripping; high-mass galaxies can better retain their gas due to the deeper potential wells (Fillingham et al. 2015). Furthermore, we refer to works such as that of Donnari et al. (2021) and Hasan et al. (2024), which investigate how galaxy properties vary with the environment using the IllustrisTNG hydrodynamical simulations, for insights from the theoretical perspective. Donnari et al. find that at low redshifts, 30 per cent of quenched group and cluster satellites were already quenched before infalling on to their current host, concluding that this is due to pre-processing for low-mass galaxies ($M_{\text{stellar}} \leq 10^{10.0-10.5} M_{\odot}$), whereas high-mass galaxies tend to quench independently of the environment or via AGN feedback. Hasan et al. also find that quenching in high-mass galaxies is driven by mass, while lower mass galaxies are more likely to be quenched in regions of higher filament linear density (i.e. thick filaments). A similar result is found by Goubert et al. (2024), suggesting

that intrinsic parameters such as black hole mass are the dominant predictor of quiescence in centrals and high-mass satellites, whereas quiescence in low-mass satellites is correlated with environmental parameters, a trend shown both in observations and simulations. This highlights the importance of considering the behaviour of both high-mass and low-mass galaxies when ascertaining the role of filaments in shaping galaxy properties.

The conclusions of this work are subject to the accuracy of our filament networks, we verify this following the reasoning of Chen et al. (2017). Filament galaxies are expected to exhibit some distinct properties. For instance, filament galaxies are expected to be more cluster-like than those in the field. A valid filament network should reflect this. To test this, we construct test networks using a completely random distribution of tracers. We find that the results presented in this work comparing filament and field galaxies vanish when using this random test network. We therefore conclude that the filament networks in this work are indeed representative of physical structure.

In this work, we are restricted to relatively high-mass galaxies. The mass limit we adopt is motivated by observational restraints. At the redshifts of the regions we study ($z \approx 0.05$), current wide-field spectroscopic surveys such as SDSS cannot provide reliable spectra for fainter low-mass galaxies. A question that we cannot answer yet is: Could lower mass galaxies show additional signatures of pre-processing not characterized by local density? A question we intend to answer through the observations collected through the WEAVE Wide-Field Cluster Survey.

5 CONCLUSIONS AND FUTURE WORK

In this work, we have investigated how the properties of 23 441 galaxies in the SDSS DR8 Main Galaxy Sample vary as a function of their environment. The stellar mass limit of our sample galaxies is $M_{\text{stellar}} > 10^{9.91} M_{\odot}$ and galaxies are selected in a narrow redshift slice about six of the WEAVE Wide-Field Cluster Survey target clusters ($z \sim 0.05$). We used DISPERSE to extract the 2D cosmic web in regions within $\sim 100 \times 100$ Mpc² area around the target clusters.

We show in Fig. 3 that galaxies inside filaments tend to be more suppressed in star formation relative to those in the field, and enhanced relative to those in groups and clusters. We find parallel trends in galaxy morphology (T-Type; Fig. 8): galaxies in filaments favour earlier type morphologies relative to the field population.

We also find that stellar mass distributions of galaxies within each environment differ, with galaxies in filaments tending to be less massive than those in cluster interiors and groups. We also find a hint that filament galaxies tend to be slightly more massive than those in the field, this difference, however, is not statistically significant. We show that when accounting for the differences in stellar mass distributions through constructing mass-matched samples, the differences in ΔSFMS (measuring star formation suppression) and T-Type persist. This is presented in Figs 5 and 9, showing that galaxies in filaments differ from those in the field and those in groups and clusters, even at fixed stellar mass. This result agrees with that of numerous past studies and suggests that galaxies in filaments are subject to pre-processing.

We have investigated whether these differences are a consequence of the well-established star formation–density and morphology–density relations by constructing mass- and local density-matched galaxy samples. While previous studies compute local densities on large scales ($> \text{Mpc}$), we compute densities on smaller scales ($\leq \text{Mpc}$) to probe the most recent, local, and stochastic physical processes. These results are presented in Figs 7 and 10. We show

that the differences between properties of galaxies in filaments and those in the field found in the mass-matched samples vanish when also matching in local galaxy density. This indicates that the effect of the filament environment can be entirely encoded within a local galaxy density index.

We find that in the mass- and density-matched samples, significant differences can only be seen when comparing cluster interiors with lower density environments. We thus conclude that the environmental effects on both star formation and morphology can be entirely characterized by local galaxy density except in the interiors of clusters. This suggests that these are unique environments, with additional physical processes such as ram-pressure stripping or strong tidal effects, which do not act significantly in other environments.

At this stage, however, we cannot make firm conclusions as to what physical processes are responsible for the results observed in this work. We think that our discussion of the possible physics is reasonable and plausible, given the available information, but speculative. However, there is a clear way forward to make progress in the future. In this work, we have focused on present-day galaxy properties such as current star formation rates and morphologies, and current environments. A natural extension would be to include temporal information through the analysis of the star formation and chemical histories of the galaxies. This is possible with the help of physically motivated galaxy evolution models, constrained with extensive photometric and spectroscopic data, such as the one presented by Zhou et al. (2022). We expect to be able to investigate and compare both star formation histories and time-scales across environments, allowing us to make firmer inferences about the physical processes at play.

The work presented here has given us very interesting insights on the effect of cosmic web filaments on the transformation of relatively massive galaxies over large spatial scales. It also serves as a precursor of the WEAVE Wide-Field Cluster Survey, where we will explore the filament and group environment in the vicinity of low-redshift clusters. The WWFCS will prove invaluable in several ways. It will, first, provide a very large and robust statistical sample containing tens of thousands of lower mass galaxies around clusters, reaching $M_{\text{stellar}} \sim 10^9 M_{\odot}$ up to $\sim 5R_{200}$ from the cluster centres. Its very high sampling density will allow us to map the cosmic web around clusters with exquisite detail. Its higher signal-to-noise spectra will yield detailed information on the star formation and stellar population properties of the galaxies, extending our current environmental research to galaxies with one order-of-magnitude smaller masses.

ACKNOWLEDGEMENTS

We thank the anonymous reviewer for their helpful comments which greatly improved the quality of this paper. The authors are indebted to Phil Parry for the technical support with the installation of DISPERSE and Daniel Cornwell whose expertise with DISPERSE helped this work immeasurably. The authors further thank Prof. Frazer Pearce whose thought-provoking comments helped to improve the quality of this paper.

This work was supported by the Science and Technology Facilities Research Council (grant number ST/X508639/1). AAS, MEG, and UK acknowledge financial support from the UK Science and Technology Facilities Council (STFC; grant ref ST/T000171/1).

Funding for SDSS-III has been provided by the Alfred P. Sloan Foundation, the Participating Institutions, the National Science Foundation, and the U.S. Department of Energy Office of Science. The SDSS-III web site is <http://www.sdss3.org/>.

SDSS-III is managed by the Astrophysical Research Consortium for the Participating Institutions of the SDSS-III Collaboration including the University of Arizona, the Brazilian Participation Group, Brookhaven National Laboratory, Carnegie Mellon University, University of Florida, the French Participation Group, the German Participation Group, Harvard University, the Instituto de Astrofísica de Canarias, the Michigan State/Notre Dame/JINA Participation Group, Johns Hopkins University, Lawrence Berkeley National Laboratory, Max Planck Institute for Astrophysics, Max Planck Institute for Extraterrestrial Physics, New Mexico State University, New York University, Ohio State University, Pennsylvania State University, University of Portsmouth, Princeton University, the Spanish Participation Group, University of Tokyo, University of Utah, Vanderbilt University, University of Virginia, University of Washington, and Yale University. For the purpose of open access, the authors have applied a Creative Commons attribution (CC BY) licence to any Author Accepted Manuscript version arising. The authors contributed to this paper in the following ways: CJO, UK, AAS, and MEG formed the core team. CJO analysed the data, produced the plots, and wrote the paper along with UK, AAS, and MEG.

DATA AVAILABILITY

The data underlying this article were accessed from SDSS DR8 <http://www.sdss3.org/dr8/>. The derived data generated in this research will be shared on request to the corresponding author.

REFERENCES

- Aihara H. et al., 2011, *ApJS*, 193, 29
 Albers S., Noble A., 2022, *Universe*, 8, 554
 Alpaslan M. et al., 2015, *MNRAS*, 451, 3249
 Aragón-Calvo M. A., van de Weygaert R., Jones B. J. T., 2010, *MNRAS*, 408, 2163
 Bahe Y. M., McCarthy I. G., Balogh M. L., Font A. S., 2013, *MNRAS*, 430, 3017
 Baldry I. K., Balogh M. L., Bower R. G., Glazebrook K., Nichol R. C., Bamford S. P., Budavari T., 2006, *MNRAS*, 373, 469
 Bamford S. P. et al., 2009, *MNRAS*, 393, 1324
 Barsanti S. et al., 2023, *MNRAS*, 526, 1613
 Blanton M. R. et al., 2005, *AJ*, 129, 2562
 Bond J. R., Kofman L., Pogosyan D., 1996, *Nature*, 380, 603
 Bond N. A., Strauss M. A., Cen R., 2010, *MNRAS*, 409, 156
 Brinchmann J., Charlot S., White S. D. M., Tremonti C., Kauffmann G., Heckman T., Brinkmann J., 2004, *MNRAS*, 351, 1151
 Brown T. et al., 2023, *ApJ*, 956, 37
 Bulichi T.-E., Dave R., Kraljic K., 2024, *MNRAS*, 529, 2595
 Castignani G. et al., 2022a, *ApJS*, 259, 43
 Castignani G. et al., 2022b, *A&A*, 657, A9
 Cautun M., van de Weygaert R., Jones B. J. T., Frenk C. S., 2014, *MNRAS*, 441, 2923
 Chen Y.-C. et al., 2017, *MNRAS*, 466, 1880
 Chung J., Kim S., Rey S.-C., Lee Y., 2021, *ApJ*, 923, 235
 Colberg J. M., Krughoff K. S., Connolly A. J., 2005, *MNRAS*, 359, 272
 Colless M. et al., 2001, *MNRAS*, 328, 1039
 Cornwell D. J. et al., 2022, *MNRAS*, 517, 1678
 Croton D. J. et al., 2006, *MNRAS*, 365, 11
 Dalton G. et al., 2014, in Ramsay S. K., McLean I. S., Takami H., eds, *Proc. SPIE Conf. Ser. Vol. 9147, Ground-Based and Airborne Instrumentation for Astronomy V*. SPIE, Bellingham, p. 91470L
 Darvish B., Sobral D., Mobasher B., Scoville N. Z., Best P., Sales L. V., Smail I., 2014, *ApJ*, 796, 51
 Darvish B., Mobasher B., Sobral D., Rettura A., Scoville N., Faisst A., Capak P., 2016, *ApJ*, 825, 113

- Domínguez Sánchez H., Huertas-Company M., Bernardi M., Tuccillo D., Fischer J. L., 2018, *MNRAS*, 476, 3661
- Donnan C. T., Tojeiro R., Kraljic K., 2022, *Nat. Astron.*, 6, 599
- Donnari M. et al., 2021, *MNRAS*, 500, 4004
- Dressler A., 1980, *ApJ*, 236, 351
- Dressler A., Oemler A., Poggianti B. M., Gladders M. D., Abramson L., Vulcani B., 2013, *ApJ*, 770, 62
- Driver S. P. et al., 2009, *Astron. Geophys.*, 50, 5
- de Vaucouleurs G., 1963, *ApJS*, 8, 31
- Eardley E. et al., 2015, *MNRAS*, 448, 3665
- Fadda D., Biviano A., Marleau F. R., Storr-Lombardi L. J., Durret F., 2008, *ApJ*, 672, L9
- Fasano G. et al., 2006, *A&A*, 445, 805
- Fillingham S. P., Cooper M. C., Wheeler C., Garrison-Kimmel S., Boylan-Kolchin M., Bullock J. S., 2015, *MNRAS*, 454, 2039
- Fujita Y., 2004, *PASJ*, 56, 29
- Galárraga-Espinosa D., Garaldi E., Kauffmann G., 2023, *A&A*, 671, A160
- Galárraga-Espinosa D. et al., 2024, *A&A*, 684, A63
- Gill S. P. D., Knebe A., Gibson B. K., 2005, *MNRAS*, 356, 1327
- Gonzalez R. E., Padilla N. E., 2010, *MNRAS*, 407, 1449
- Goubert P. H., Bluck A. F. L., Piotrowska J. M., Maiolino R., 2024, *MNRAS*, 528, 4891
- Gunn J. E., Gott J. R. III, 1972, *ApJ*, 176, 1
- Haas M. R., Schaye J., Jeon-Daniel A., 2012, *MNRAS*, 419, 2133
- Hasan F. et al., 2023, *ApJ*, 950, 114
- Hasan F. et al., 2024, *ApJ*, 970, 177
- Hashimoto Y., Augustus Oemler J., Lin H., Tucker D. L., 1998, *ApJ*, 499, 589
- Hinshaw G. et al., 2013, *ApJS*, 208, 19
- Hoosain M. et al., 2024, *MNRAS*, 528, 4139
- Jackson J. C., 1972, *MNRAS*, 156, 1P
- Jin S. et al., 2024, *MNRAS*, 530, 2688
- Kaiser N., 1984, *ApJ*, 284, L9
- Kauffmann G. et al., 2003, *MNRAS*, 341, 33
- Kauffmann G., White S. D. M., Heckman T. M., Ménard B., Brinchmann J., Charlot S., Tremonti C., Brinkmann J., 2004, *MNRAS*, 353, 713
- Kim S. et al., 2016, *ApJ*, 833, 207
- Kleiner D., Pimblet K. A., Jones D. H., Koribalski B. S., Serra P., 2017, *MNRAS*, 466, 4692
- Kotecha S. et al., 2022, *MNRAS*, 512, 926
- Kraljic K. et al., 2018, *MNRAS*, 474, 547
- Kuchner U. et al., 2020, *MNRAS*, 494, 5473
- Kuchner U. et al., 2021a, *MNRAS*, 503, 2065
- Kuchner U. et al., 2021b, *MNRAS*, 510, 581
- Kuutma T., Tamm A., Tempel E., 2017, *A&A*, 600, L6
- Laigle C. et al., 2018, *MNRAS*, 474, 5437
- Larson R. B., 1974, *MNRAS*, 169, 229
- Larson R. B., Tinsley B. M., Caldwell C. N., 1980, *ApJ*, 237, 692
- Libeskind N. I. et al., 2018, *MNRAS*, 473, 1195
- Lu Y. S., Mandelker N., Oh S. P., Dekel A., van den Bosch F. C., Springel V., Nagai D., van de Voort F., 2024, *MNRAS*, 527, 11256
- Luber N., Van Gorkom J. H., Hess K. M., Pisano D. J., Fernández X., Momjian E., 2019, *AJ*, 157, 254
- McGee S. L., Balogh M. L., Bower R. G., Font A. S., McCarthy I. G., 2009, *MNRAS*, 400, 937
- Mahajan S., Singh A., Shobhana D., 2018, *MNRAS*, 478, 4336
- Malavasi N. et al., 2017, *MNRAS*, 465, 3817
- Martínez H. J., Muriel H., Coenda V., 2016, *MNRAS*, 455, 127
- Moore B., Katz N., Lake G., Dressler A., Oemler A., 1996, *Nature*, 379, 613
- Moretti A. et al., 2017, *A&A*, 599, A81
- Muldrew S. I. et al., 2012, *MNRAS*, 419, 2670
- Nair P. B., Abraham R. G., 2010, *ApJS*, 186, 427
- Nulsen P. E. J., 1982, *MNRAS*, 198, 1007
- Oesch P. A. et al., 2010, *ApJ*, 714, L47
- Oyarzun G. A., Bundy K., Westfall K. B., Lacerna I., Yan R., Brownstein J. R., Drory N., Lane R. R., 2023, *ApJ*, 947, 13
- Parente M. et al., 2024, *ApJ*, 966, 154
- Peng Y.-j. et al., 2010, *ApJ*, 721, 193
- Pimblet K. A., Drinkwater M. J., Hawkrigg M. C., 2004, *MNRAS*, 354, L61
- Poggianti B. M. et al., 2017, *ApJ*, 844, 48
- Popesso P. et al., 2011, *A&A*, 532, A145
- Ramsøy M., Slyz A., Devriendt J., Laigle C., Dubois Y., 2021, *MNRAS*, 502, 351
- Ricciardelli E., Cava A., Varela J., Tamone A., 2017, *ApJ*, 846, L4
- Salim S. et al., 2007, *ApJS*, 173, 267
- Sampaio V. M., De Carvalho R. R., Ferreras I., Aragón-Salamanca A., Parker L. C., 2022, *MNRAS*, 509, 567
- Sarron F., Adami C., Durret F., Laigle C., 2019, *A&A*, 632, A49
- Scholz-Díaz L., Martín-Navarro I., Falcón-Barroso J., 2022, *MNRAS*, 511, 4900
- Singh A., Mahajan S., Bagla J. S., 2020, *MNRAS*, 497, 2265
- Snedden A., Coughlin J., Phillips L. A., Mathews G., Suh I.-S., 2016, *MNRAS*, 455, 2804
- Sobral D., Best P. N., Smail I., Geach J. E., Cirasuolo M., Garn T., Dalton G. B., 2011, *MNRAS*, 411, 675
- Song H. et al., 2021, *MNRAS*, 501, 4635
- Sousbie T., 2011, *MNRAS*, 414, 350
- Strauss M. A. et al., 2002, *AJ*, 124, 1810
- Szpila J., Davé R., Rennehan D., Cui W., Hough R., 2024, preprint ([arXiv:2402.08729](https://arxiv.org/abs/2402.08729))
- Thomas D., Maraston C., Bender R., Mendes de Oliveira C., 2005, *ApJ*, 621, 673
- Thompson B. B., Smith R., Kraljic K., 2023, *MNRAS*, 518, 1361
- Trussler J., Maiolino R., Maraston C., Peng Y., Thomas D., Goddard D., Lian J., 2020, *MNRAS*, 491, 5406
- Vulcani B. et al., 2019, *MNRAS*, 487, 2278
- Vulcani B. et al., 2020, *ApJ*, 892, 146
- Vulcani B., Poggianti B. M., Smith R., Moretti A., Jaffe Y., Gullieuszk M., Fritz J., Bellhouse C., 2022, *ApJ*, 927, 91
- Wang K., Wang X., Chen Y., 2023, *ApJ*, 951, 66
- Wang W. et al., 2024, *MNRAS*, 532, 4604
- Wolf C. et al., 2009, *MNRAS*, 393, 1302
- Wu J. F., Jespersen C. K., Wechsler R. H., 2024, preprint ([arXiv:2402.07995](https://arxiv.org/abs/2402.07995))
- Yang X., Mo H. J., van den Bosch F. C., Pasquali A., Li C., Barden M., 2007, *ApJ*, 671, 153
- York D. G. et al., 2000, *AJ*, 120, 1579
- Zel'dovich Y. B., 1970, *A&A*, 5, 84
- Zhou S., Merrifield M., Aragón-Salamanca A., Brownstein J. R., Drory N., Yan R., Lane R. R., 2022, *MNRAS*, 517, 3723
- Zhou S., Aragón-Salamanca A., Merrifield M., 2024, *MNRAS*, 530, 4082

This paper has been typeset from a $\text{\TeX}/\text{\LaTeX}$ file prepared by the author.